Stony Brook University

Remote Angular Measurement of Flat Targets

A Thesis Presented
by

Neha Aggarwal

to

The Graduate School
in Partial Fulfillment of the
Requirements
for the degree of

Master of Science
in
Electrical Engineering

Stony Brook University
May 2012

Stony Brook University
The Graduate School

Neha Aggarwal

We, the thesis committee for the above candidate for the
Master of Science degree, hereby recommend
acceptance of this thesis.

Dr. Harbans Dhadwal, Thesis Advisor,
Associate Professor, Electrical and Computer Engineering Department

Dr. Muralidhara Subbarao,
Professor, Electrical and Computer Engineering Department

This thesis is accepted by the Graduate School.

Charles Taber,

Interim Dean of the Graduate School

Abstract of the Thesis

Remote Angular Measurement of Flat Targets

by

Neha Aggarwal

Master of Science

in

Electrical Engineering

Stony Brook University

2012

This report presents a method for the remote measurement of angular position of flat surfaces, especially focussing on improving the accuracy of the measured angle. The technique is based on obtaining the temporal signature of non-linear, reflecting image patterns that are printed on to the surface of the target. The system uses a laser scanning system for reading a bar pattern, which can be represented by a pulse position modulation scheme. Angular orientation can be measured upto the distance of one meter.

The complete angle measurement system comprises of a laser scanning section and a photodiode receiver which provides the raw signal which is processed by a 32-bit microcontroller using an analog to digital converter and a time base counter. The recovered digital signal from the analog to digital converter is processed to recover the rotational angle of a flat surface at a

distance of 1 meter from the scanning mirror. The system has a measured angular resolution which is better than $\pm 0.005^0$ over a 2^0 span when the printed bars are having the initial orientation from the vertical axis greater than 80^0 with respect to horizontal scanning axis. The angular resolution is $\pm 0.05^0$ for an absolute angle measurement in the range of -85^0 to $+85^0$.

To My Parents

Sham Lal Aggarwal and Saroj Aggarwal

and my beloved brother

Ankush

Table of Contents

List of Figures

List of Tables

ACKNOWLEDGEMENTS

This thesis would have never been possible without the support and help of numerous people. I would like to begin by thanking my advisor Professor Harbans Dhadwal who has been a great mentor throughout the process of working on this project. He always found time to solve my queries in his busy schedule. His tactness and resourcefulness has always inspired me to think beyond my limitations. Without his immense support and belief, it would have never been possible to overcome the various experimental challenges.

Financial Support from Omnitek Partners is sincerely appreciated. I would like to extend my gratitude to my committee member, Professor Muralidhara Subbarao, for taking time off his busy schedule to examine my thesis report and give valuable advice. I would also like to thank my colleague, Shih Hsi Yen(Jason) who has been a good friend to me and also helped by giving insightful suggestions from time to time. I would have never been able to write this report without my friend Suhas Mysore Satheesh. I would like to thank him for providing the latex templates and explaining things.

I would like to express my deepest gratitude towards my parents and my beloved brother in India for their incessant support and encouragement in all the decisions of my life.

Chapter 1

Introduction

Precise angle measurement is critical to the operation of many diverse systems, found in applications ranging from the aircraft altitude to the orientation of robots. Speed and accuracy are key factors along with the adaptability to the outside environment.

Various optical methods have been presented, due to non-contact, high sensitivity and high resolution such as autocollimator[1][2][3], interferometer[4][5], differential detection based on internal-reflection effect[6], total internal multi-reflection[7], and the moire technique[8]. The interferometer is based on the principle of the interference of two laser beams that traverse slightly different optical paths whenever an angular displacement occurs whereas an autocollimator measures an angular displacement by detecting the lateral displacement of a laser beam reflected from a mirror that is subjected to the angular displacement. Interferometer and autocollimator can provide higher accuracy among these existing methods. However, it is often very difficult to integrate these methods with machines because of their large size. In contrast, differen-

tial detection, based on internal reflection effect, can make devices very stable, compact, and easily adaptable for a broad range of scan distance. In total internal multi-reflection, the semiconductor laser with single-mode fiber affords the stable illumination beam, and the beam expander induces a gain factor enlarging the small angular displacement, thus improving the angle measurement sensitivity and stability simultaneously. However, most of these methods require careful consideration of transmitter and receiver location which makes it difficult to implement in open environments.

Despite of all these techniques, there exists a need for remote angular measuring systems, especially for the military application. In general, remote angle measurement systems can be used to recover the linear velocity and/or rotational velocity, and thereby the acceleration of an object relative to a reference system at one or more positions of the object trajectory during its motion. The relevance of this technique is discussed in a patent[9]. To provide the initial absolute position and orientation and the related velocity information to accelerometers and gyros mounted on an object for the purpose of allowing such accelerometers and gyros to determine the angle of the object. To accomplish this, it is required to provide a sensory system, i.e., sensors and their instrumentation that do not require the mounting of sensors on the object, and do not interfere with the operation of the object[9].

The main focus of this thesis is in the design and fabrication of a system for measuring the rotation angle for flat surface, elevation and azimuth angles for cylindrical object. The measurements are to be performed at a distance of one

meter from the scanning mirror. A commercial laser scanner, from Motorola Systems, formed the basis of the first generation system, which did not meet the required resolution needs. Subsequently, laser scan engine was replaced by a new design which is described in this thesis report.

1.1 Previous Work

The work presented in this thesis is the continuation of the work done by Daichi Horimai[10]. The primary goal of fabricating the angle measurement device for rotation angle for flat surface, elevation and azimuth angle for cylindrical object with a distance of 1 meter has been done by using *commercial barcode scanner SE960HP, microcontroller and a printed bar pattern*. The bar patterns printed on the flat surface and cylindrical object was successful at sending its information about the rotation, elevation and azimuth angle, in the range of $\pm 5^0$ and $\pm 10^0$ for flat surface and cylindrical object, respectively.

When the steps were taken to increase the precision of the measured rotation angle, and elevation and azimuth angle for flat surface and cylindrical object, respectively, new problems were faced. It was observed that a lot of noise was being produced, primarily because of the SE960HP commercial laser scanner.

The main reasons for not using SE960HP commercial laser scanner furthermore, are described below:

1. The signal from the scanner was the output of a comparator which was generating random glitches in between the original data. The random

glitches could have been reduced by adjusting the threshold of the comparator but there was no mechanism provided to do so. Moreover, there were no other test points provided on the laser scanner so that the raw reflected signal could be recovered for post processing using custom designed hardware.

2. The spot size of the SE960HP laser scanner was approximately 5mm, which was too large for measuring a small change in the width of bar pattern. This system could not be adapted for detecting angular changes of the order of a few milliradians at one meter distance.

3. The concept of measuring the change in angle is based upon the change in width when the angle of the target surface is changed. So, it is very important to observe the consistent width at one position. To verify this functionality, 50 test runs had been done at a specific position with no change in the surrounding parameters. Width of bar pattern was measured in terms of number of counts from the microcontroller. It can be analysed from the fig 1.1, 1.2, 1.3 and 1.4 that the observed is inconsistent over the number of runs.

Thus, it was determined the system specifications were not enough to achieve the required precision and a new approach was taken which is described in this thesis report. Basic theory used is still the same as described in chapter 2 but the hardware implementation change is described in chapter 3.

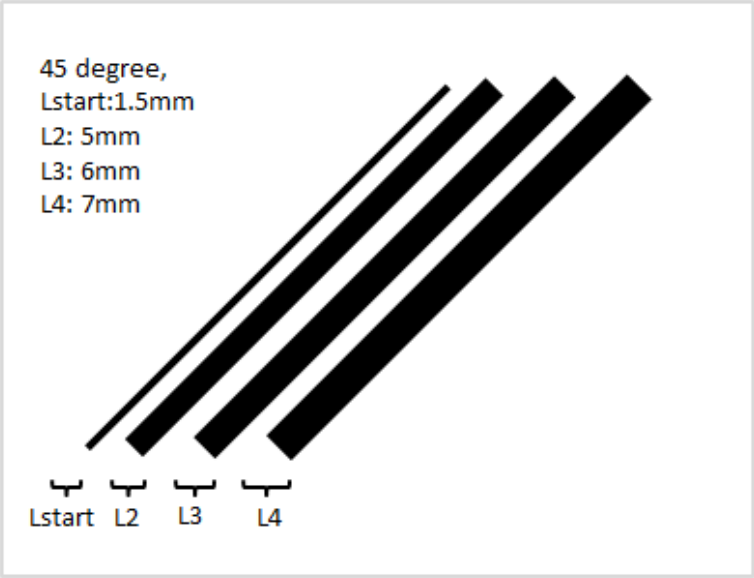

Figure 1.1: Bar pattern used to observe the consistency of measured width at one position with bars of 5mm, 6mm and 7mm at 45 degree angle

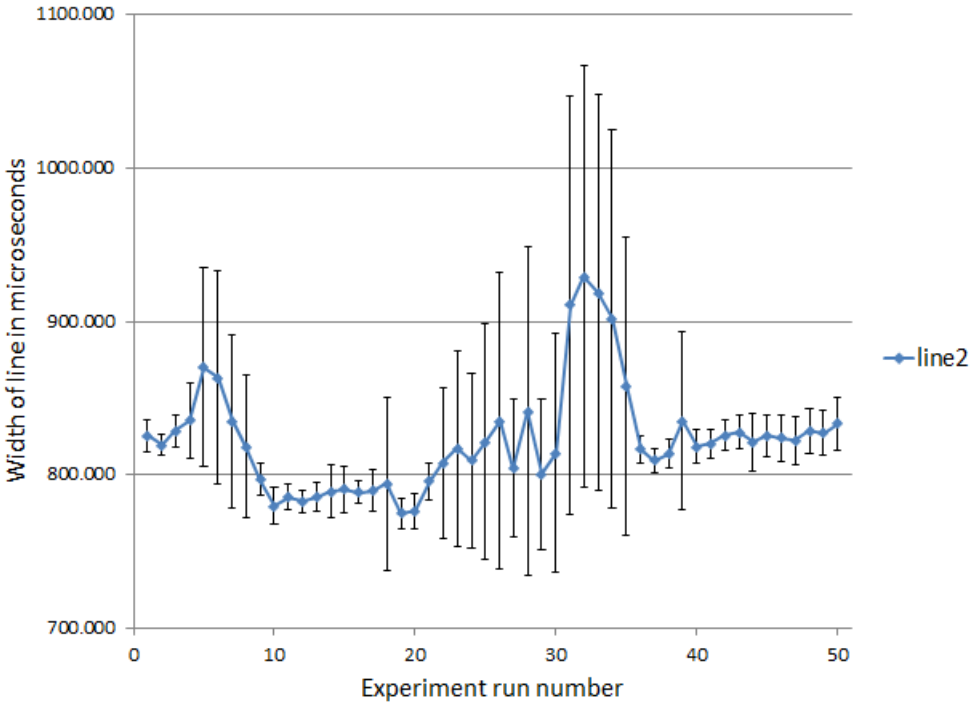

Figure 1.2: Observed width of line 2 in Figure1.1

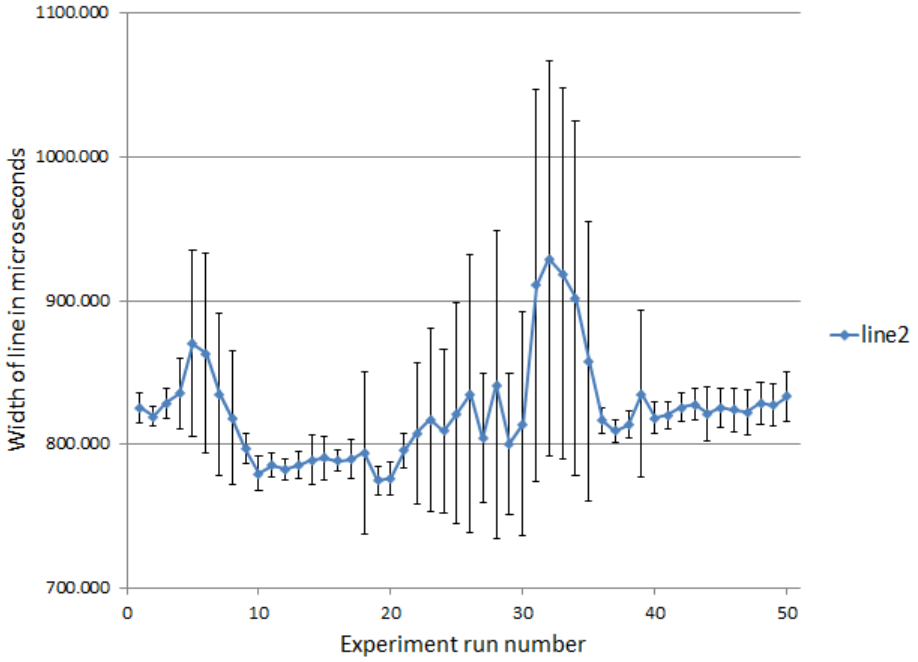

Figure 1.3: Observed width of line 3 in Figure1.1

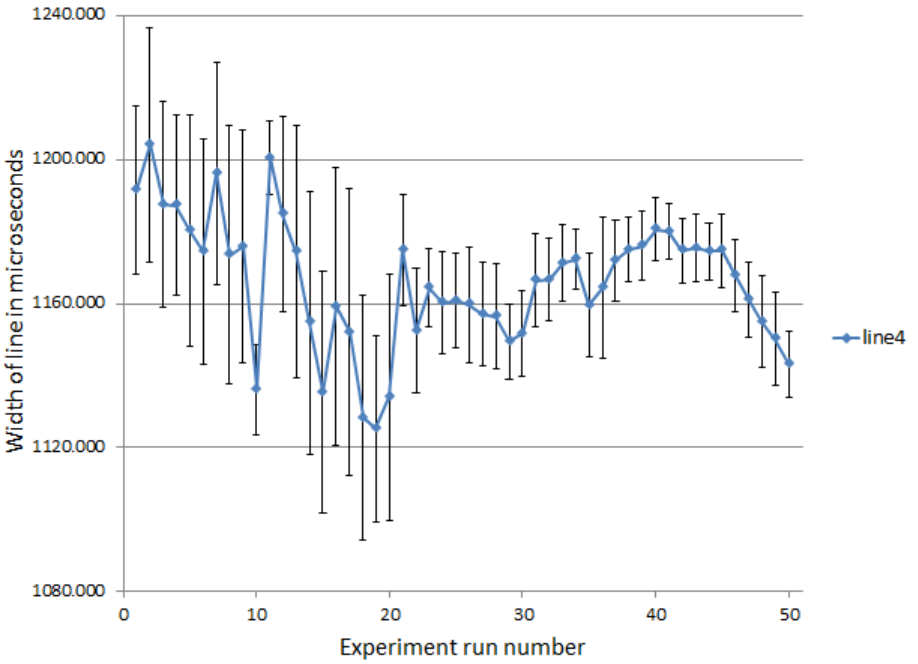

Figure 1.4: Observed width of line 4 in Figure1.1

Chapter 2

Theoritical Background

The angular measurement technique is based on obtaining a temporal signature of a non-linear, diffused reflecting image that is printed or engraved on to the surface of the target. Angular position measurement can be achieved at a distance of one meter, for illustrative purpose the analysis below uses a one-dimensional scanning system for reading a bar pattern, which can be represented by a pulse position modulation scheme[10].

At first glance this pattern may be mistaken for the ubiquitous bar code found on all products, and an incorrect inference that bar code scanning solution may be tailored to meet the needs of an angular displacement sensor. However, this would be an incorrect observation as the similarity ends with shape of the bar, a bar code comprises of a sequence of fixed width space marks which can either be dark or white, corresponding to a digital 1s or 0s. Scanning and non-scanning (imaging) systems are used for detection of the sequence of 1s and 0s representing the product numeric code. The emphasis of such system is on the recovery of the digital sequence from arbitrary ori-

entation of the bar codes. Such systems cannot be easily adapted for angular measurement[10].

A new signal processing technique has been proposed on a scanning based system to get the required angular information. A laser beam illuminates the target and a retro-reflective optical system provides the instantaneous temporal signature of the target bar pattern in Figure 2.1.

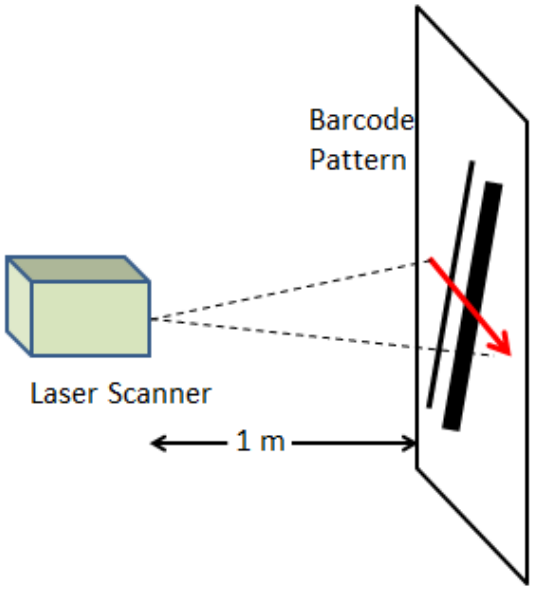

Figure 2.1: Barcode scanner scans the bar pattern on flat surface horizontally

The retro-reflective target can be characterized by a spatial distribution f(x), which for example could be sequence of rectangular functions

$f(x) = \sum_j rect[\frac{x - X_{oj}}{W_{oj}}]$ where,

X_{oj} = Position of the j^{th} bar in the pattern

W_{oj}= Width of the j^{th} bar in the pattern

2.1 Calculating rotation angle in flat surface

As the laser spot movers across the target it generates a time varying signal. The signal will vary depending on the frequency at which scanning mirror is operated along with the amplitude as scan length varies with amplitude. The 0^0 rotating angle signal, v(t,0) and θ^0 rotation angle signal v(t,θ) is shown in the Figure 2.2 and 2.3.

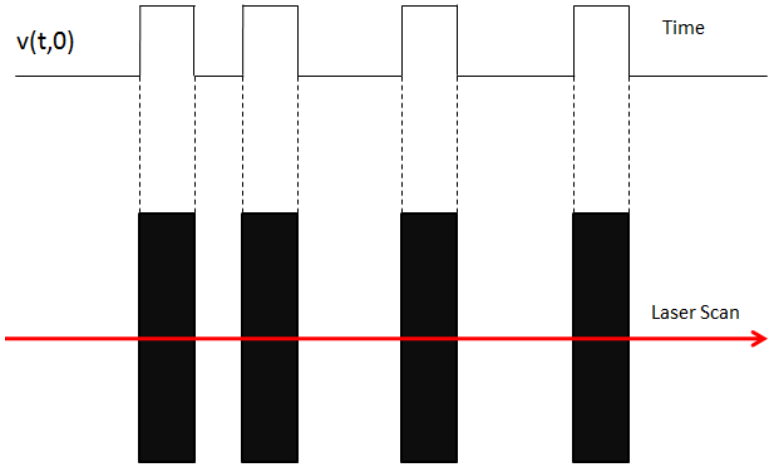

Figure 2.2: Rotating angle signal v(t,0) produced by scanning by laser scan at 0 degree angle

In the following equations the subscript j has been dropped for clarity. The rotation angle can be recovered from the width of bar W(θ) using the transformation

$\theta = cos^{-1}[\frac{W(0)}{(V)(T(\theta))}]$ where,

W(0) is the the initial width of the bar,

v is the scan velocity at the bar location and

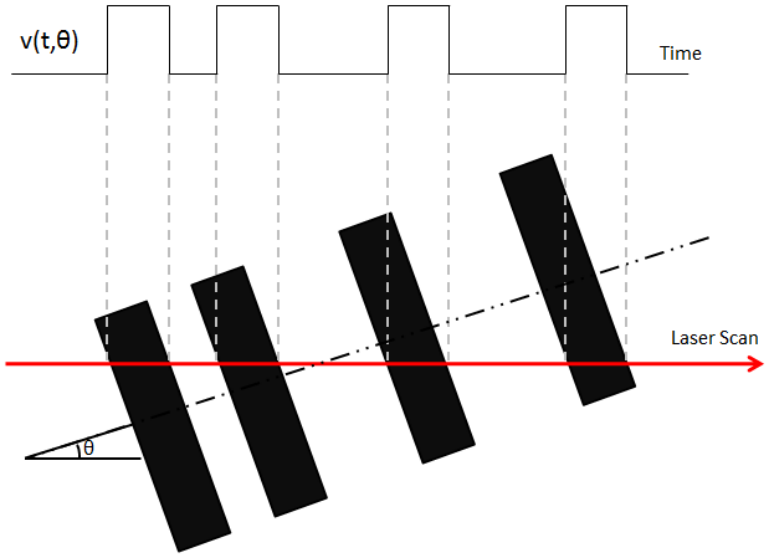

Figure 2.3: Rotating angle signal v(t,θ) produced by scanning by laser scan at θ degree rotation angle

ΔT is the measured time width of the bar

This measurement requires knowledge of the scan velocity which is not constant throughout the scan. It is possible to compute a correction for the velocity error which is described in following section 5.1.

The velocity error will effect in the case of absolute angle measurement and dependence on velocity can be eliminated by normalizing the time measurement with a reference time measurement made at say θ=0, giving

$$\frac{cos(\theta+\Delta\theta)}{cos(\theta)} = \frac{[\frac{W(0)}{(V)(T(\theta+\Delta\theta))}]}{[\frac{W(0)}{(V)(T(\theta))}]} = \frac{T(\theta)}{T(\theta+\Delta\theta)}$$

$$cos(\theta+\Delta\theta) = (cos(\theta))(\frac{T(\theta)}{T(\theta+\Delta\theta)})$$

$$\Rightarrow \Delta\theta = cos^{-1}[(cos(\theta))(\frac{T(\theta)}{T(\theta+\Delta\theta)})] - \theta$$

Thus, to measure the differential change in angle, the initial absolute angle θ should be known.

Chapter 3

Hardware implementation and setup

The main hardware components used in this thesis report are transmitter(having laser and laser diode driver circuitry), biconvex lens used to focus the beam coming out of fiber optic cable, scanning mirror set at 45^0 relative to incoming beam, receiver section(having photodiode,current sensitive preamplifier and voltage sensitive amplifier), micro-controller to process the signal coming out of receiving circuitry, and target bar pattern. All components are carefully selected to meet the goals of this project.

3.1 Transmitter

The transmitter circuitry used in this project consists of two major components, *a laser diode* and *a laser diode driver*. Various types of laser diodes and drivers are available in the market. The components used here are described below:

3.1.1 Laser Diode(LD)

A 658nm wavelength laser diode from Thor Labs[11](LPS-660-sf20) with an ouput power(P_o) of 20mW is used for the scanning source. The laser diode is pigtailed to a single mode optical fiber modeled with a mode field diameter of 4.6μm.

Figure 3.1: Laser diode's emitted light focused into an angled ferrule of a fiber

The Figure 3.1 shows a schematic of the commercial coupling arrangement employed to maximize the throughput by minimizing reflections. The angled facet(8^0) at the proximal end of the fiber reduces specular reflections from re-entering the laser diode. If this reflected light were reflected back towards the diode, light would be coupled into the diode causing fluctuations in power and wavelength.

The specifications of the laser are shown in table 3.1 and the drawings showing the side view, bottom view and pin diagram are shown in Figure 3.2.

3.1.2 Laser Diode Driver(LDD)

Laser diodes require careful handling as they can be easily destroyed by the electrostatic discharges. The laser diode driver design must include a soft

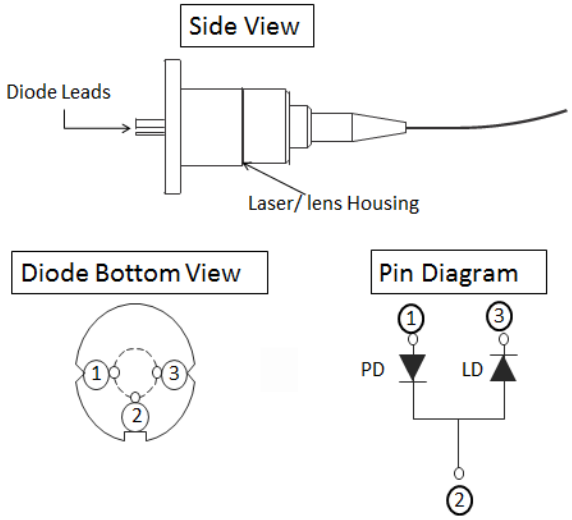

Figure 3.2: Drawings of LP660-SF20 - 658 nm, 20 mW, A Pin Code, SM Fiber Pigtailed Laser Diode

Specification	**Min.**	**Typ.**	**Max.**
wavelength	655nm	658nm	665nm
threshold current*	-	40mA	55mA
slope efficiency*	0.35	0.47	-
operating current @$P_o = 20mW$*	-	80mA	110mA
operating voltage @$P_o = 20mW$*	-	2.6V	3.0V
monitor current @$P_o = 20mW$*	0.1mA	0.3mA	0.6mA

*Temperature=25^0C.

Table 3.1: Optical Electrical Characteristics

start/shut down capability to extend laser diode life. Due to recent proliferation of laser diodes in the marketplace, many commercial laser diode drivers are available to meet many diverse requirements. The LDD M laser diode driver from Wavelength Electronics[12] offers many unique features. These include:

- 200 mA output current drive capacity

- Constant power stability < 0.02% typical (24 hours ambient)
- Single supply operation: +5 V to +12 V
- Operates in constant current or constant power mode
- Isolated, buffered current and power measurement outputs
- 12-turn trimpot controls output current or power
- Eight pins solder to PCB
- Output current slow starts when V+ is applied
- The 1M and 3M Modules can be operated from a negative supply if the laser diode anode needs to be earth grounded.

3.1.2.1 Pin Description

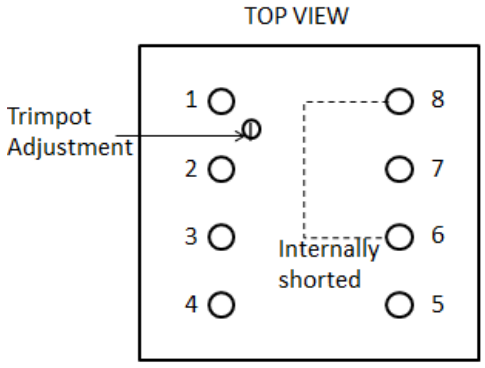

Figure 3.3: Top View of LDDPCB-3M

1. **Trimpot Adjustment:** The trimpot adjusts the laser diode forward current setting in constant current mode and the photodiode current setting in constant power mode.

2. **Pin 1 Current Monitor:** In Constant Power Mode, this output is used to monitor the current through the laser diode. The transfer function in constant power mode is 80 mA/Volt. In Constant Current Mode, this pin must be tied to pin 7. Pin 2 then becomes the laser diode current monitor (80 mA/Volt).

3. **Pin 2 Power Monitor** In Constant Power Mode, this output is used to monitor the photodiode current. The transfer function for a 1M is 1000 mA/Volt. In Constant Current Mode, this output is used to monitor the laser diode forward current. The laser diode current transfer function is 80 mA/Volt.

4. **Pin 3 ON/OFF** Once power (V+) is applied across pins 8 and 4, pin 3 can be used to enable or disable the laser diode current. The output will be enabled if pin 3 floats or is grounded. If pin 3 is tied to V+, the output will be disabled and the laser diode current will be reduced to a standby state ($\leq$ 5 mA in constant current mode or the equivalent of 5 mA or 15 mA of photodiode current in constant power mode). Do not disconnect or connect the laser diode to the driver in the standby state.

5. **Pin 4 GND** This and pin 8 (V+) provide power to the control electronics and laser diode output.

6. **Pin 5 Laser Diode Cathode**

7. **Pin 6 Laser Diode Anode** This pin is internally shorted to pin 8 (V+). Do not connect this pin to earth ground when pin 4 (GND) is connected to earth ground. Since pin 8 (V+) and pin 6 (LD ANODE) are internally shorted, this will result in shorting out the power supply connected to the LDD M driver. If the laser diode anode and the power supply ground are both required to be earth grounded, you will need to operate the 1M from a negative power supply.

8. **Pin 7 Photodiode Anode** This pin is attached to the photodiode anode for constant power mode operation. This pin must be shorted to pin 1 (Current Monitor) to operate in constant current mode. Remove any photodiode connections from pin 7 in constant current mode.

9. **Pin 8 V+** This pin is internally shorted to pin 6 (Laser Diode Anode). This pin provides power to the control electronics and laser diode output. The LDD M Series has internal control circuitry which turns the output on and off depending on the voltage at pin 8 (V+). When the voltage reaches the power up trip point (4.9 Volts), the module soft starts the laser diode. The soft start ramp is approximately 100 msec. If pin 3 (ON/OFF) is floating or grounded, the output current will be determined by the setting of the adjustment trimpot. When the voltage reaches the power down trip point (4.2 Volts), the module shunts current around the laser diode, powering it down in a controlled fashion.

3.1.2.2 Operating Instructions

Good connections are important for safe and optimum performance of the M series module. There are three modes of operation for this laser driver diode module: *Constant Current Mode*, *Constant Power Mode* and *Operation when laser diode must be earth grounded*. In this report, laser diode driver has been used in constant current mode with laser diode anode/photodiode cathode common configuration and appropriate connections has been made through steps described below.

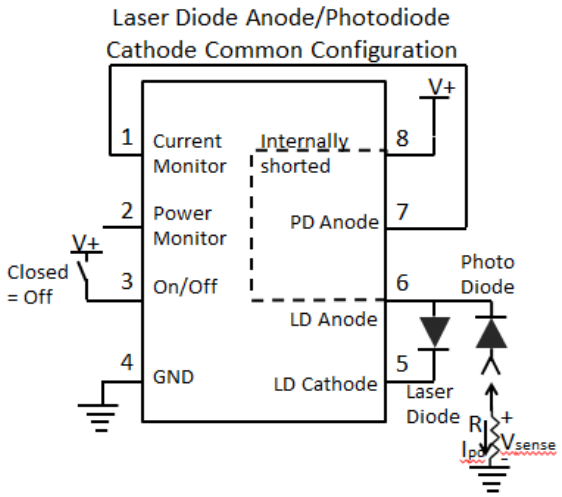

Figure 3.4: Laser Diode Configuration Connections in Constant Current Mode

1. Jumper pin 1 and 7 and connect the laser diode to pin 5 and 6. The photodiode is optional. If you need to monitor the photodiode current(I_{pd}) while in constant current mode, attach the photodiode as shown in the Figure 3.4. For photodiode currents greater than 100μA, choose R equal

to 1KΩ. For photodiode currents less than 100μA, choose R equal to 10KΩ. $I_{pd} = V_{sense}/R$

2. Before attaching the power supply to the LDD, preset the supply voltage between +5 and +12V. With the power supply unplugged from AC, attach the power supply output to pins 8 and 4.

3. Either ground pin 3, leave it floating, or use a switch as shown in the Figure 3.4. Turn the output current trimpot fully counter clockwise. Do not slowly increase the voltage from the power supply; this may damage the Laser Diode and Driver. Apply power to the unit.

4. Use a digital voltmeter to monitor Pin 2. This is the Current Monitor for constant current mode operation. The transfer function is 80mA/Volt.

5. *Exceeding maximum laser diode operating current* $[I_{OP}]$ *will damage your laser diode.* Begin with the output adjust trimpot turned fully counter-clockwise. Adjust the output current trimpot **slowly** clockwise until the voltage at pin 2 corresponds to desired laser diode current $[I_{OP}]$. The trimpot rotates through 12 turns between 0mA and 200mA.

3.2 Imaging System

A biconvex or plano convex lens is used to project a magnified image of the source, integrated fiber optic light probe(IFOLP)[13], on to the target as shown in Figure3.5. IFOLP is a cluster of optical fibres with one single mode fiber

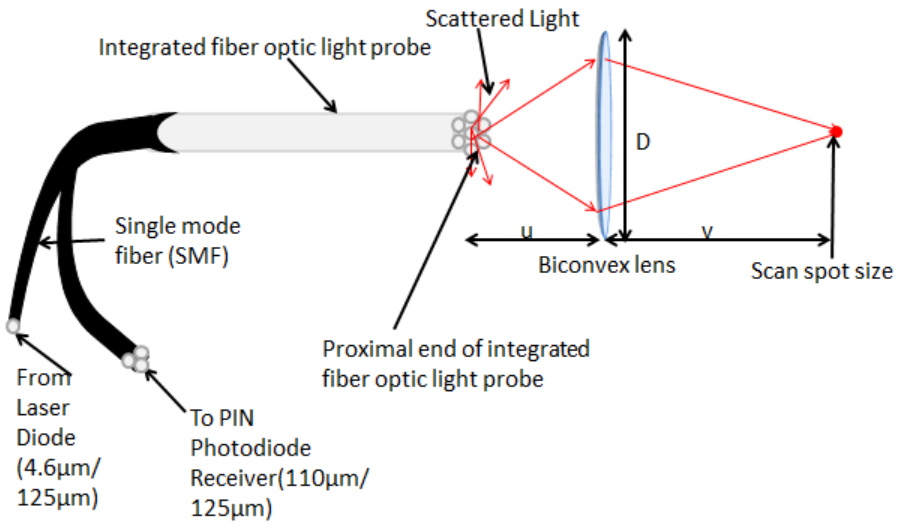

Figure 3.5: Illustration of magnified imaging through integrated light probe and biconvex lens

from laser diode surrounded by multi-mode fibers receiving retro-reflective light from target. The multi-mode mode fibers transmits the diffused reflected raw signal to PIN photodiode. The mode field to cladding ratio for single mode and core to cladding ration for multi-mode fiber is shown in Figure3.5. Focal length of lens is calculated as follows:

Magnification of lens, M $=\frac{D_I}{D_S} = \frac{v}{u}$ where,

D_I is size of image(1mm)

D_S is size of source(10μm)

v is distance of image(100cm) and

u is distance of source

Therefore, M=10=$\frac{v}{u}, \Rightarrow \frac{1}{u} = \frac{10}{v}$

Now, using $\frac{1}{u} + \frac{1}{v} = \frac{1}{f}$

$\Rightarrow$ **f=9.0cm**

3.3 Scanning Mirror

3.3.1 General Operation

The one dimensional optical scanning device employs a G330 optical scanner with a 26x26mm scanning mirror made by General Scanning Inc[14]. The light beam falling on the scanning mirror is the reflected onto the target bar pattern.

The G330 scanner is driven by a signal generator. The coil configuration is shown in Figure 3.6. For proper operation the black and yellow wires must be connected, as must the red and green.

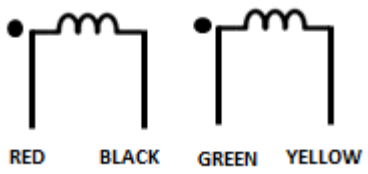

Figure 3.6: G330 scanner coil configuration

3.3.2 Scanning Angle Calibration

It has been found experimentally that the optimum signal generator frequency is 130Hz, that is, the frequency at which maximum scanning angle occurs for a fixed amplitude driving voltage. At the optimum frequency, we varied the driving voltage amplitude and measured the scanning distance. The experimental set used is shown in Figure 3.7. The distance d, from the scanning mirror to the target is 1m.

The data obtained by performing the above experiment is tabulated in

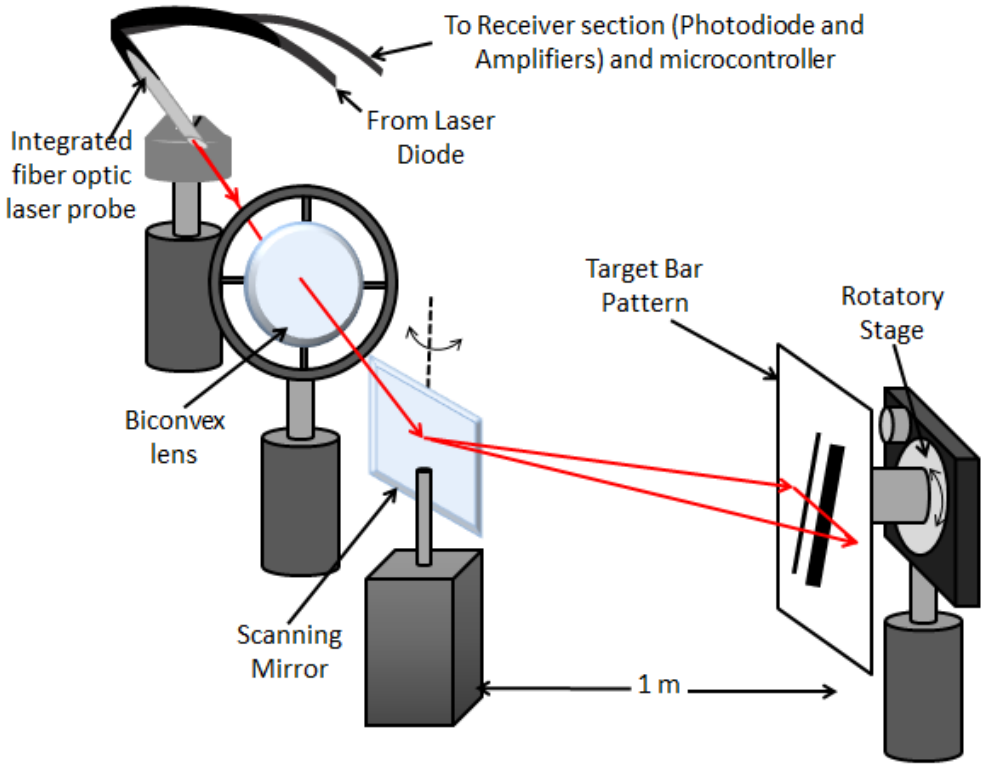

Figure 3.7: Experimental setup used to calibrate the scanner

table 3.2. V is the rms voltage of the signal generator measured in volts and D is the scanning distance measured in cm.

The experiments using G330 scanner having 26x26mm with target bar pattern at 0.5m are giving good results. The intensity of received signal reflected by the target bar pattern is approximately -40dBm, at a distance of 50cm. It drops to -45dBm approximately when the distance is increased to 1meter, causing the decoder to fail. The scanning mirror is replaced with a mirror of 75x75mm dimensions, boosting the intensity of the received signal to -38.56dBm. The larger scanning mirror required re-calibration of the scan

V(volts)	D(cm)
0.8	15.5
0.85	16.4
0.90	17.4
0.95	18.4
1.0	19.5
1.5	29.5
2.0	39.8
2.5	49.4
3.0	60.2
3.5	70.8
4.0	81.7
4.5	92.8
5.0	103

Table 3.2: Experimental data (Voltage vs Distance) obtained by experiment shown in 3.7

angle. The optimum signal generator frequency with G330 scanning device having a 75x75mm scanning mirror is 40Hz, primarily due to the increased weight. At the optimum frequency, the scan length varies with the amplitude.

3.4 Receiver

This section consists of a photodiode, current sensitive pre-amplifier and a low noise voltage amplifier.

3.4.1 Photodiode Receiver

The diffusely scattered light from the target is collected by a ring of receiving optic fibers, surrounding the single mode source fiber[13]. The distal end of the

receiving optical fiber is terminated in a SMA connector which is connected to a PIN photodiode receiver. Figure3.8 shows a schematic of optical receiver and

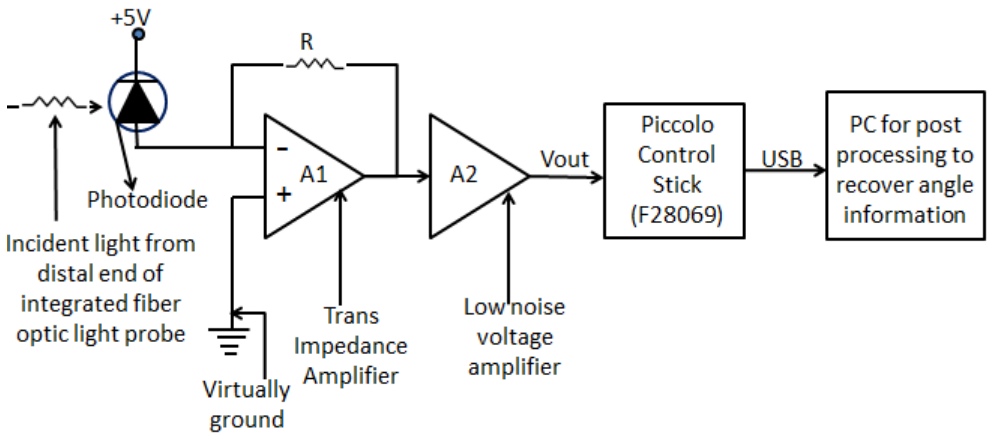

Figure 3.8: A schematic of optical receiver and data acquisition system based on Piccolo microcontroller

data acquisition system based on 32-bit piccolo microcontroller(f28069)[15]. A photodiode is a type of photodetector capable of converting light into either current or voltage, depending upon the mode of operation which are described below.

3.4.1.1 Principle of operation

A photodiode is a p-n junction or PIN structure. When a photon of sufficient energy strikes the diode, it excites an electron, thereby creating a free electron (and a positively charged electron hole). This mechanism is also known as the *inner photoelectric effect*. If the absorption occurs in the junction's depletion region, or one diffusion length away from it, these carriers are swept from the junction by the built-in field of the depletion region. Thus holes move toward

the anode, and electrons toward the cathode, and a photocurrent is produced. This photocurrent is the sum of both the dark current (without light) and the light current, so the dark current must be minimized to enhance the sensitivity of the device[16].

3.4.1.2 Mode of operation

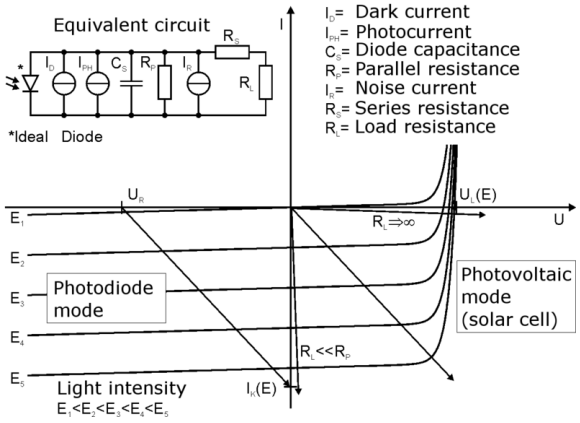

Figure 3.9: Graph illustrating the modes of operation of Photodiode

Photovoltaic mode When used in zero bias or photovoltaic mode, the flow of photocurrent out of the device is restricted and a voltage builds up. This mode exploits the photovoltaic effect.

Photoconductive mode In this mode the diode is often reverse biased (with the cathode positive), dramatically reducing the response time at the expense of increased noise. This increases the width of the depletion layer, which decreases the junction's capacitance resulting in faster response times. The reverse bias induces only a small amount of current (known

as saturation or back current) along its direction while the photocurrent remains virtually the same. For a given spectral distribution, the photocurrent is linearly proportional to the illuminance (and to the irradiance).

Other modes of operation Avalanche photodiodes have a similar structure to regular photodiodes, but they are operated with much higher reverse bias. This allows each photo-generated carrier to be multiplied by avalanche breakdown, resulting in internal gain within the photodiode, which increases the effective responsivity of the device.

3.4.2 Current Sensitive Preamplifier

As an optical photodiode is a current source, producing the current proportional to the illuminating light intensity. Therefore, it is ideally suited to a trans-impedance amplifier(TIA) configuration as shown in Figure3.8. In this report, the Model 1642 Current amplifier[17] is used which is a simple, low cost, wide band gain block for use with photodiode multipliers, photodiode detectors, and other current source type inducers. It operates with an input virtual ground to mitigate the effects of source and cabling shunt capacitance and to prevent loading effect on non-linear transducers such as photodiodes.

An input offset trimpot can be used to prevent unwanted current from upsetting the zero bias voltage condition of a quiescent photodiode detector, or alternatively to trim the output voltage to zero.

3.4.3 Low Noise Voltage Preamplifier

The Model 1201 Voltage Preamplifier[18] with Remote Gain Programming Option is usable in both computer controlled and manual applications, but in this project, it has been controlled manually to give a gain to signal from the output of current sensitive preamplifier as shown in Figure3.8. In addition to gain status, low pass and high pass filter outputs are also available which can be used if required.

3.5 Laser Barcode Scanner

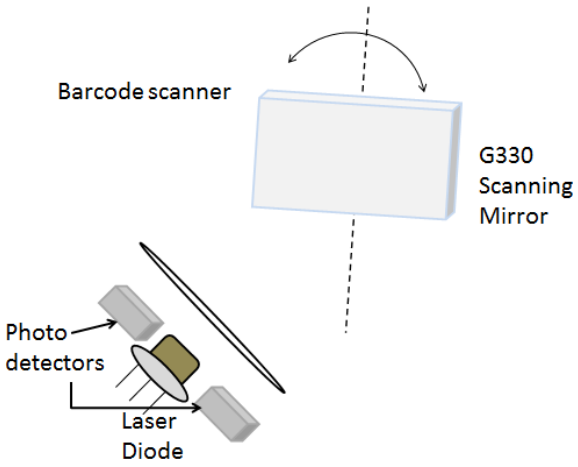

Figure 3.10: Diagram showing basic components of a laser barcode scanner

This section brings together the various subsystems described in the sections 3.1, 3.2 and 3.3. A laser comprises of three modules, 1) a laser beam source, 2) scan generating optics, mirror and lens, and 3) optical receiver. This section explains how the laser type barcode scanner scans and reads the barcode. The optical fiber transmitting the laser beam also contains the photo

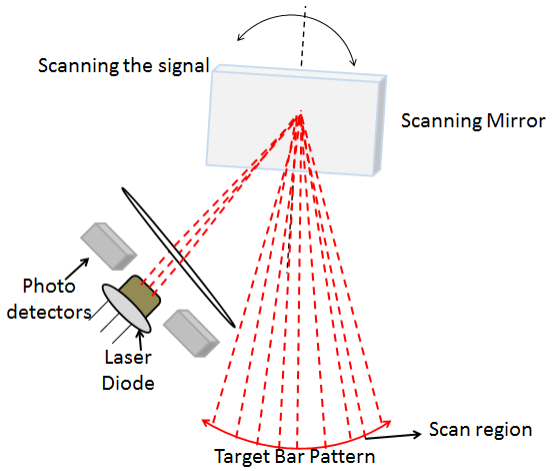

Figure 3.11: Illustration showing the retro-reflective laser scanner scans the bar pattern. Laser diode emits the laser beam collimated by biconvex lens towards mirror, in certain scanning angle

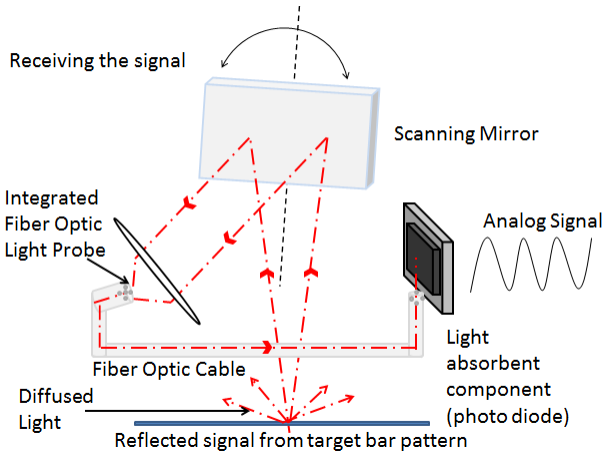

Figure 3.12: Illustration showing the retro-reflective laser barcode scanner receives the signal through an integrated fiber optic light probe trans-receiver

receptors to receive the reflected signal by the target bar pattern which will be sent to the light absorbent component or photodiode. Thus, the scanning system is mainly comprised of a laser diode and a scanning mirror and can be simply shown as in Figure 3.10.

Collimated laser beam coming from the convex lens to the scanning mirror driven at the optimum scanner frequency is on left and right reciprocating motion. The laser will be reflected by a mirror and do the scanning left and right as shown in Figure 3.11.

(a) Bar Pattern 1

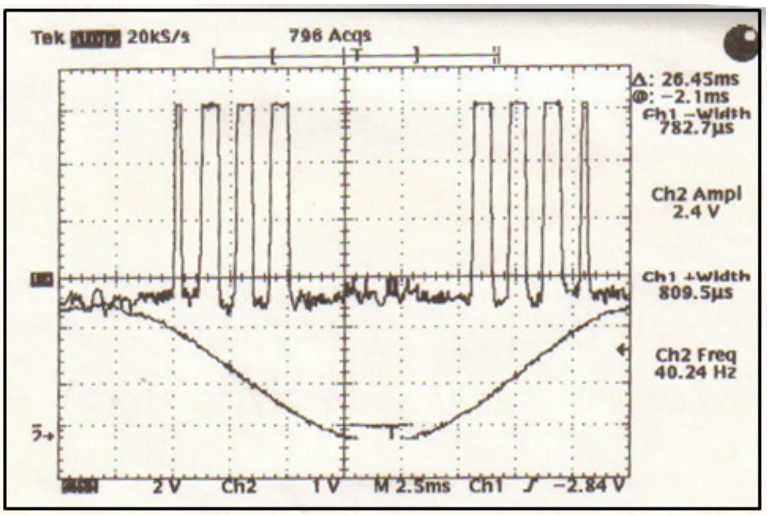

(b) Received analog signal 1

Figure 3.13: Received analog signal(1) after processing through receiver section with (a) showing the bar pattern used and (b) showing the received signal on CRO

Collimated laser beam is reflected by the scanning mirror towards the target bar pattern. The diffused reflected light will again be received by the laser photo receptors and sent to the absorbent component or photodiode through the optical fiber. The absorbed diffused reflected light will convert the light reflection strength into an electrical analog signal as shown in Figure 3.12.

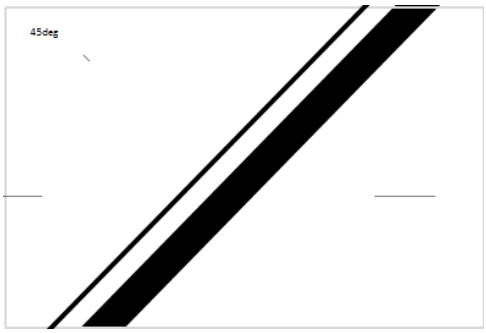

(a) Bar Pattern 2

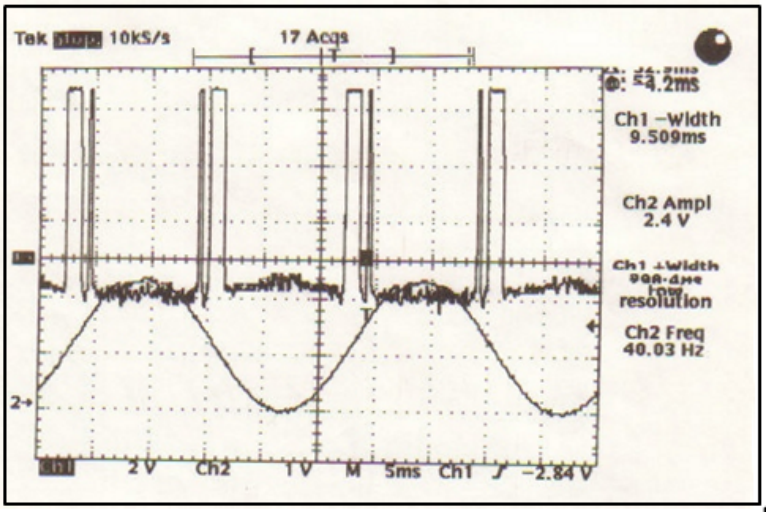

(b) Received analog signal 2

Figure 3.14: Received analog signal(2) after processing through receiver section with (a) showing the bar pattern used and (b) showing the received signal on CRO

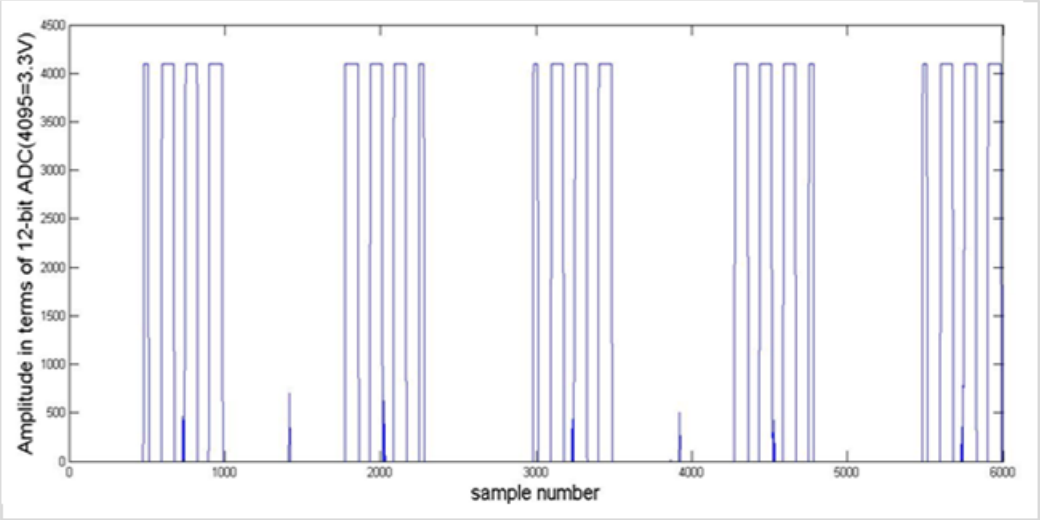

(a) Digital Signal 1

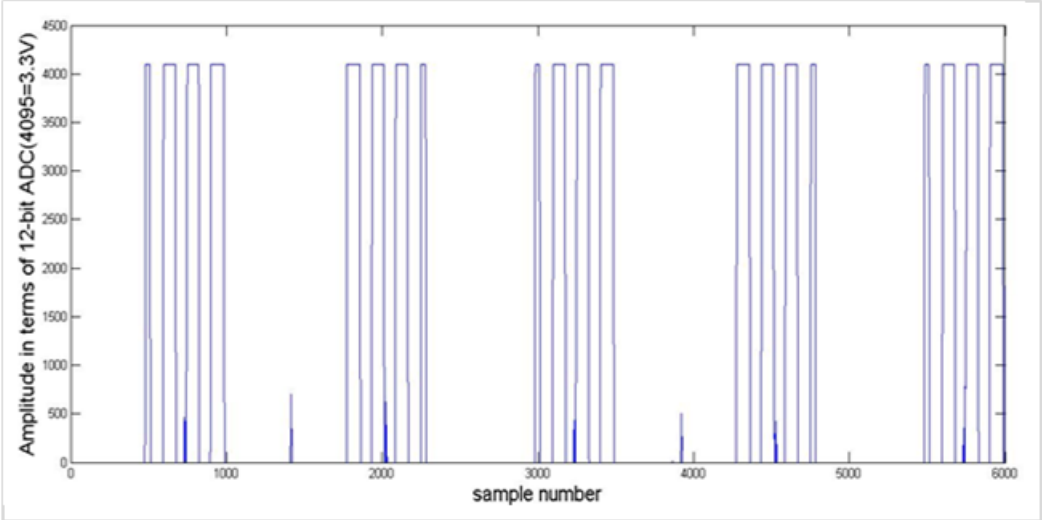

(b) Digital Signal 2

Figure 3.15: Recovered digital signal after processing through ADC with (a) showing the digital signal 1 and (b) showing the digital signal 2 (plotted through matlab) corresponding to Figure 3.13 and Figure 3.14, respectively

The received analog signal will then be passed through the preamplifier and

a low pass filter. The received analog signal after processing through receiver section is as shown in Figure 3.13(b) and 3.14(b). It can been seen in received signal graph, channel 1 output corresponds to the data bar pattern.Also, there is a DC-offset which has been kept so that the noise from the edges will not interfere with the actual information which is collected by 12-bit analog to digital converter at 3.3 Volts. Also, the channel 2 output shows the sine wave of 40.2 Hz which is used to drive the scanning mirror.

The analog signal is converted into a digital signal as shown in Figure 3.15 using a 12 bit analog to digital converter of piccolo F28069 microcontroller which is described in next section 3.6.

3.6 Piccolo Microcontroller F28069

Piccolo control stick[15] allows quick and easy evaluation all of the advanced capabilities of Texas Instruments Piccolo microcontroller TMS320F28069. Slightly larger than a memory stick, the Piccolo control stick features on board JTAG emulation and access to all control peripherals.

3.6.1 Features of TMS320F28069 Microcontroller

Following features of TMS320F28069 are used in this project[15]:

1. High-Efficiency 32-Bit CPU
    - 80 MHz (12.5-ns Cycle Time)
    - 16 x 16 and 32 x 32 MAC Operations

- 16 x 16 Dual MAC
- Harvard Bus Architecture
- Atomic Operations
- Fast Interrupt Response and Processing
- Unified Memory Programming Model
- Code-Efficient (in C/C++ and Assembly)

2. Clocking
   - Two Internal Zero-pin Oscillators
   - On-Chip Crystal Oscillator/External Clock Input
   - Dynamic PLL Ratio Changes Supported
   - Watchdog Timer Module
3. Three 32-Bit CPU Timers
4. Up to 8 Enhanced Pulse Width Modulator(ePWM) Modules
5. 12-Bit ADC, Dual Sample-and-Hold
   - Up to 3 MSPS
   - Up to 16 Channels

3.6.2 Description of Analog to Digital Converter

This section includes the detailed description of 12-bit ADC according to which their respective register bits can be modified[19].

3.6.2.1 Features

The core of the ADC contains a single 12-bit converter fed by two sample and hold circuits. The sample and hold circuits can be sampled simultaneously or sequentially. These, in turn, are fed by a total of up to 16 analog input channels. See the device datasheet for the specific number of channels available. The converter can be configured to run with an internal bandgap reference to create true-voltage based conversions or with a pair of external voltage references (VREFHI/LO) to create ratiometric based conversions. Functions of the ADC module include[19]:

1. 12-bit ADC core with built-in dual sample-and-hold (S/H)
2. Simultaneous sampling or sequential sampling modes
3. Full range analog input: 0 V to 3.3 V fixed, or VREFHI/VREFLO ratiometric
4. Up to 16-channel, multiplexed inputs
5. 16 SOCs, configurable for trigger, sample window, and channel
6. 16 result registers (individually addressable) to store conversion values
7. Multiple trigger sources such as software immediate start, ePWM 1-8, CPU timers 0/1/2, ADCINT1/2.

3.6.2.2 SOC(start of conversion) Principle of Operation

SOC is configuration set defining the single conversion of a single channel. In that set there are three configurations: the trigger source that starts the conversion, the channel to convert, and the acquisition (sample) window size. Each SOC is independently configured and can have any combination of the trigger, channel, and sample window size available. Multiple SOCs can be configured for the same trigger, channel, and/or acquisition window as desired. This provides a very flexible means of configurating conversions ranging from individual samples of different channels with different triggers, to oversampling the same channel using a single trigger, to creating your own series of conversions of different channels all from a single trigger.

3.6.2.3 ADC Conversion Priority

When multiple SOC flags are set at the same time, one of two forms of priority determines the order in which they are converted. The default priority method is round robin. In this scheme, no SOC has an inherent higher priority than another. Priority depends on the round robin pointer (RRPOINTER)which points to the last SOC converted. The highest priority SOC is given to the next value greater than the RRPOINTER value, wrapping around back to SOC0 after SOC15. At reset the value is 32 since 0 indicates a conversion has already occurred. When RRPOINTER equals 32 the highest priority is given to SOC0.

The whole process with an example is described in Figure 3.16 for bet-

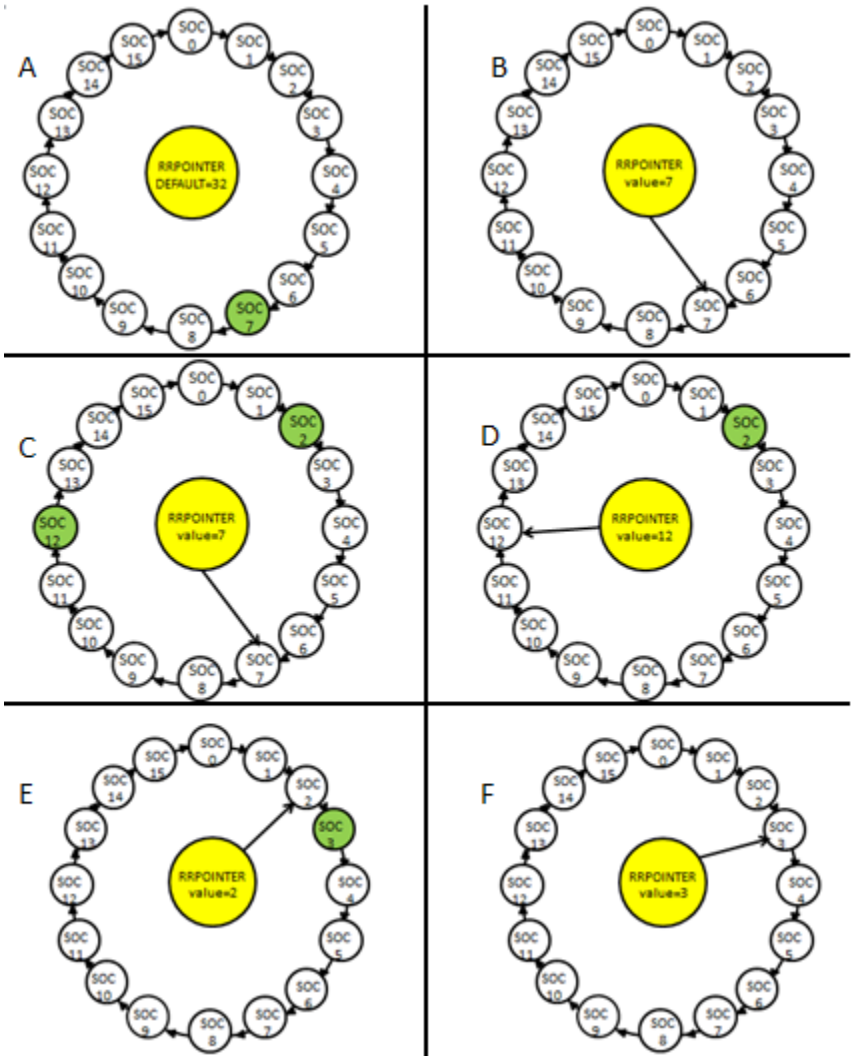

Figure 3.16: Round Robin Priority Example

ter understanding. In Figure 3.16(A), after reset default RRPOINTER is 32 and SOC0 is highest priority SOC. SOC7 receives trigger and it's configured channel is converted immediately. Figure 3.16(B), RRPOINTER changes to point to SOC7 as this is the last converted SOC. SOC8 is now the highest priority SOC. Figure 3.16(C), SOC2 and SOC12 triggers are received at the

same time. Since SOC12 is first on the round robin wheel, it's channel is converted while SOC2 remains pending. Figure 3.16(D), RRPOINTER changes to SOC12 and SOC2 channel is converted. SOC3 is at highest priority now. Figure 3.16(E), RRPOINTER changes to 2 and SOC3 receives trigger and it's channel is converted. Figure 3.16(F), RRPOINTER points to 3 and SOC4 is at highest priority in round robin wheel.

3.6.2.4 End of Conversion (EOC)

Just as there are 16 independent SOCx configuration sets, there are 16 EOCx pulses. In sequential sampling mode, the EOCx is associated directly with the SOCx. In simultaneous sampling mode, the even and the following odd EOCx pair are associated with the even and the following odd SOCx pair. The ADC contains 9 interrupts that can be flagged and/or passed on to the PIE. Each of these interrupts can be configured to accept any of the available EOCx signals as its source. The configuration of which EOCx is the source is done in the INTSELxNy registers. Additionally, the ADCINT1 and ADCINT2 signals can be configured to generate an SOCx trigger. This is beneficial to creating a continuous stream of conversions.

3.6.2.5 Internal Reference Voltage Selection

The ADC can operate in two different reference modes, selected by the ADCCTL1.ADCREFSEL bit. By default the internal bandgap is chosen to generate the reference voltage for the ADC. This will convert the voltage presented according to a fixed scale 0 to 3.3v range. The equation governing conversions

in this mode is:

Digital Value = 0, when Input $\leq$ 0v

Digital Value = 4096 [(Input VREFLO)/3.3v], when 0v<Input<3.3v

Digital Value = 4095, when Input $\geq$ 3.3v

$*$All fractional values are truncated

$**$VREFLO must be tied to ground in this mode.

3.6.3 Description of Enhanced Pulse Width Modulation

An enhanced PWM[19] peripheral must be able to generate complex pulse width waveforms with minimal CPU overhead or intervention. It needs to be highly programmable and very flexible while being easy to understand and use. The ePWM unit described here addresses these requirements by allocating all needed timing and control resources on a per PWM channel basis. Cross coupling or sharing of resources has been avoided; instead, the ePWM is built up from smaller single channel modules with separate resources that can operate together as required to form a system. This modular approach results in an orthogonal architecture and provides a more transparent view of the peripheral structure, helping users to understand its operation quickly. Each ePWM module supports the following features[19]:

1. Dedicated 16-bit time-base counter with period and frequency control
2. Two PWM outputs that can be used in the following configurations:
    - Two independent PWM outputs with single-edge operation

- Two independent PWM outputs with dual-edge symmetric operation
- One independent PWM output with dual-edge asymmetric operation

3. Asynchronous override control of PWM signals through software
4. Programmable phase-control support for lag or lead operation relative to other ePWM modules
5. Hardware-locked (synchronized) phase relationship on a cycle-by-cycle basis
6. Dead-band generation with independent rising and falling edge delay control
7. Programmable trip zone allocation of both cycle-by-cycle trip and one-shot trip on fault conditions
8. A trip condition can force either high, low, or high-impedance state logic levels at PWM outputs
9. All events can trigger both CPU interrupts and ADC start of conversion (SOC)
10. Programmable event prescaling minimizes CPU overhead on interrupts
11. PWM chopping by high-frequency carrier signal, useful for pulse transformer gate drives

In this project, ePWM has been used as a time base module(TB) which has following configuration parameters[19]:

1. Scale the time-base clock (TBCLK) relative to the system clock (SYSCLK-OUT).
2. ConFigure the PWM time-base counter (TBCTR) frequency or period.
3. Set the mode for the time-base counter:
    - count-up mode: used for asymmetric PWM
    - count-down mode: used for asymmetric PWM
    - count-up-and-down mode: used for symmetric PWM
4. ConFigure the time-base phase relative to another ePWM module
5. Synchronize the time-base counter between modules through hardware or software
6. ConFigure the direction (up or down) of the time-base counter after a synchronization event.
7. ConFigure how the time-base counter will behave when the device is halted by an emulator
8. Specify the source for the synchronization output of the ePWM module:
    - Synchronization input signal
    - Time-base counter equal to zero

- Time-base counter equal to counter-compare B (CMPB)
- No output synchronization signal generated

3.7 Observation Target

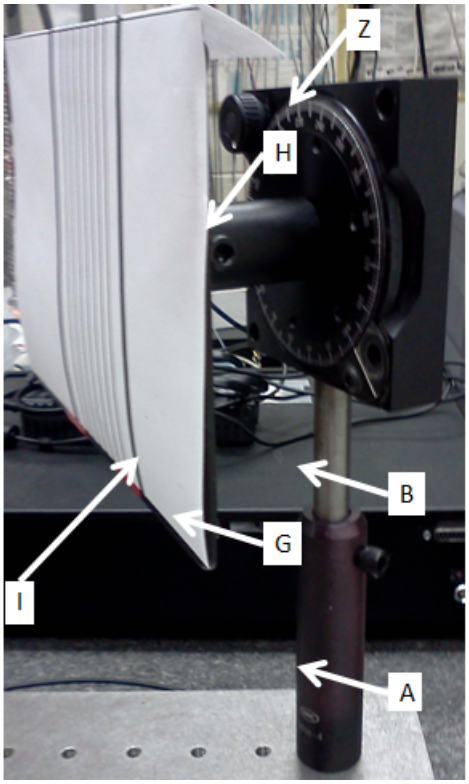

A: (Newport) Model:VPH-4
Vertical Post Holder 4 inch

B: (Newport) Model:9623
Stainless Steel Post, 4.0 in. Height,
0.5 in. Diameter

Z: (Newport) Model: RSX-2
Rotation Stage

G: Plastic board
(155mm x 120mm)

H: (Newport) Model: VPH-2
Standard Post Holder, 2 in. Height,
0.5 in. Diameter Post

I: Printed Barcode Pattern

Figure 3.17: Components used for flat surface rotation angle measurement

Flat surface is used as a target to calculate the rotation angle. The barcode pattern is printed on the surface and taped on the surface towards the barcode scanner located at a distance of 1 meter in order to analyze the difference in angle measurement with different distances to see the accuracy of the measurement.

For the flat surface rotation angle measurement, a plastic board with a size of 150mm width and 115mm height is placed at the rotating stage as shown in the Figure 3.17. This stage has a resolution of 2 degree and is rotated manually.

3.7.1 Print Contrast Signal (PCS)

The laser scanner reads the barcode by collecting the light that is diffused and scattered from the target. A barcode with a strong contrast between the background and the print ink is easy to read. Conversely, if the contrast is less than 10dB then the barcode is difficult to read[10].

The standard that gives the strength of this diffused reflection is called Print Contrast Signal (PCS). PCS can be determined from reflectance ratio of the space Rs, and the reflectance ratio of the line Rl, followed by equation below:

$$PCS = [\frac{Rs-Rl}{Rs}]$$

From the equation above, if the space is completely white and the reflectance ratio is nearest to 100%, and if the line is completely black and the reflectance ratio is as nearest to 0%, PCS will be 1. As this explains, the barcode that has the PCS close to 1 is the barcode that is easy to read. Therefore, the scanner friendly barcode must to be printed on white paper and line should be printed as dense as possible. If the barcode pattern is printed to the white paper using ink jet printer, it might cause reading error as shown in the Figure 3.18[10].

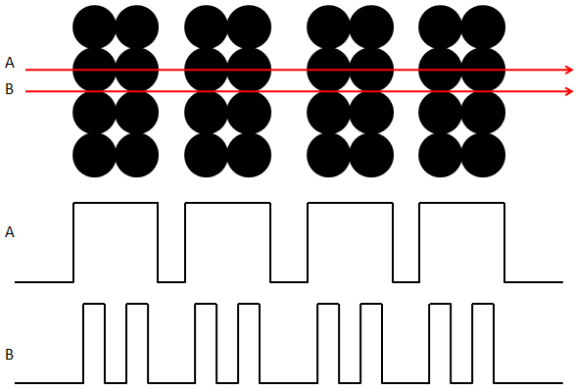

Figure 3.18: A is the appropriate signal from printed bar pattern and output signal. B is the different output signal caused by the dots by the inkjet printer

In practise the bar pattern with a PCS value close to unity can be printed with a high resolution printer, for example, 1200x600 dpi. The Mean Reflective Difference (MRD) is an alternative metric to PCS is defined by the difference between the reflectance rate of the bars and spaces.

3.7.2 Difference in bar reading with surface color

Visible laser diode at 658nm is used in this project. The Figure 3.19 shows the reflectance of various spectral wavelength against various target color. For 658nm visible laser diode, purple, blue, or green has low reflectance, and yellow, orange, or red has higher reflectance. The lowest reflectance color is black and the highest reflectance color is white[10].

As shown in the Figure 3.19, red, yellow, or orange color surface as high reflectance so it can be recognized as white (space), and blue, green, or purple has lower reflectance so it can be recognized as black (bar). Therefore,at a scan wavelength of 658nm, the highest contrast is obtained with a blue bar on

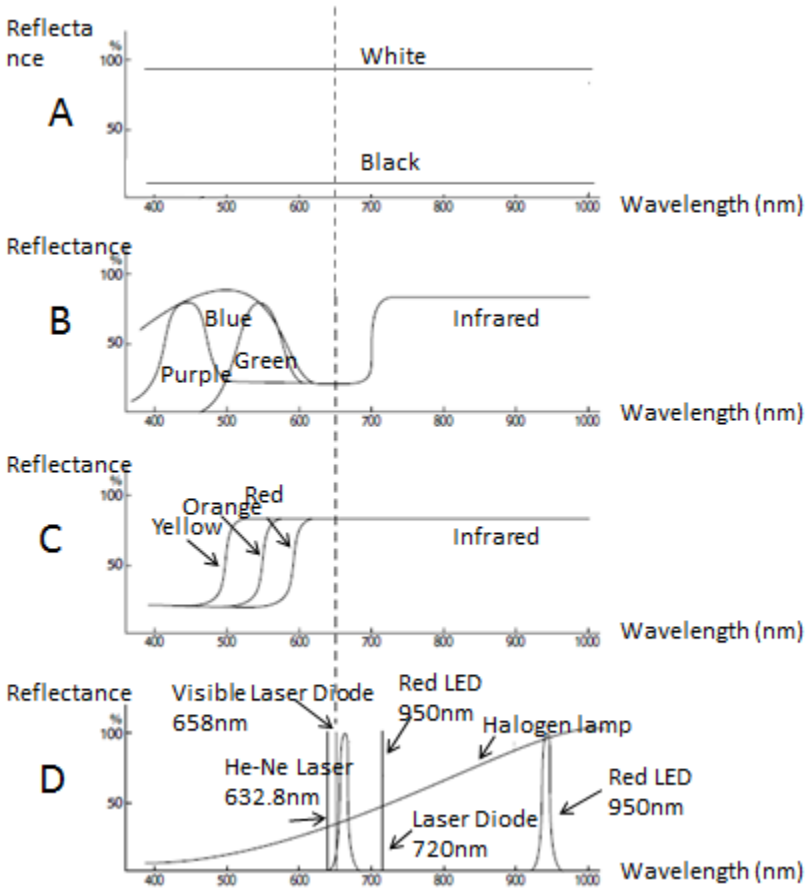

Figure 3.19: Reflectance Curve due to several target color versus each light source wavelength (Figure[D]). For 658nm visible laser diode, Figure[B] shows lower reflectance at purple, blue, or green surface color, and Figure[C] shows high reflectance at yellow, orange, or red surface color. Figure[A] shows white has high reflectance and black has low reflectance for any wavelength.

a white background, black bar on a red background or purple bar on a yellow background. The lowest contrast, and therefore unreadable, combination to be avoided is a red bar on a white background or black bar on a blue background.

3.8 Bar Pattern

To get the accurate result from the barcode scanner, the target pattern must be designed to send the appropriate signal to the barcode scanner.

3.8.1 Start signal, main pattern, and quiet zone

The barcode pattern consists of three parts, start signal, main pattern, and quiet zone as in Figure 3.20. Start signal is the marker that barcode scanner sends the microcontroller where to start reading the barcode pattern as next bar will be the actual data. The microcontroller is programmed to ignore any error signals, arising from surface imperfections. Main pattern represents the valid data which microcontroller uses for comparing the signal between the initial and final state of the surface. As the scanning mirror does two scans, left to right and right to left, in each period of the sinusoidal frequency at which it operates, the start signal also works as the stop signal.

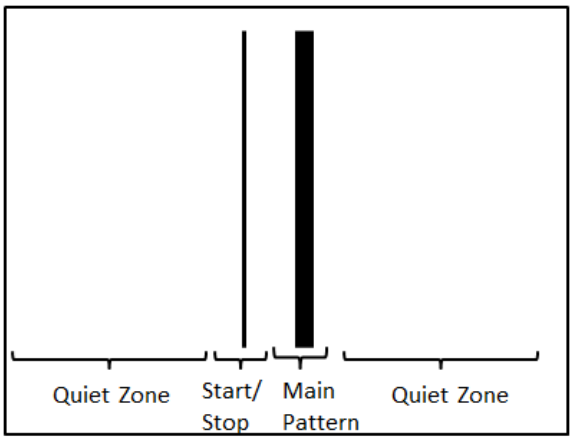

Figure 3.20: Bar pattern

3.8.2 Bar line and space width

The barcode pattern used in this experiment is given in the Figure 3.21. The start line (Lstart) is both 1.5mm, start space (Start)is 12mm. Main pattern consists of 1 line (L1) with 5mm width line. As the ADC sampling frequency can be changed manually through the software, it has been found that minimum line width that can be successfully decoded is 0.5mm.

During a typical scan, the lines are rotated at 45 degree from the vertical. As described in chapter2 the change in width follows a cosine law, which predicts an increase in angular resolutions at larger inclination angles. The width information is extracted from the measured analog signal by using a dual threshold as discussed in section3.5. Voltage levels greater than 3.3V corresponds to "1" and those below 0V corresponds to "0". A level shifter is employed to filter the background noise from the voltage signal.

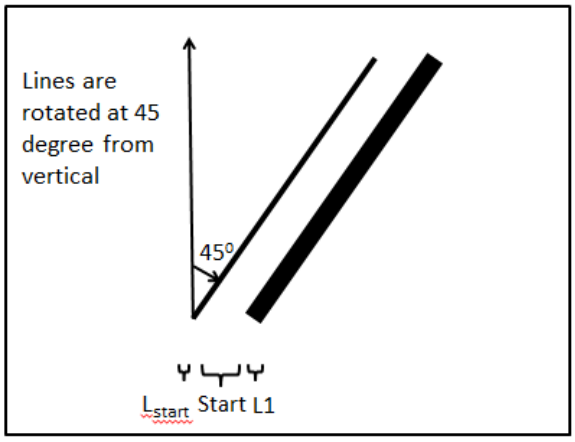

Figure 3.21: Line and space widths of the bar pattern used in the experiment

Chapter 4

Software Setup

Microcontroller TMS320F28069 converts the raw analog data from the receiving circuitry to digital data using the 12-bit ADC. The stored digital signal information is then processed to obtain the width of the bars on the target bar pattern from which angle is calculated as described in the chapter 2. As the ADC digitizes the signal between 0-3.3 Volts; some random glitches occurring between bars are also filtered out. Threshold for the start bar is required to be adjusted in the software as the sampling frequency for analog to digital converter varies.

4.1 Flow Chart

The ePWM parameters includes an up counter and time base period register which is going to determine the sampling frequency of ADC. A SOC interrupt is generated whenever up counter values is equal to the time base period register and the ADC samples the input analog signal. ADC samples are stored in an array which approximately includes 10 scans if time base counter

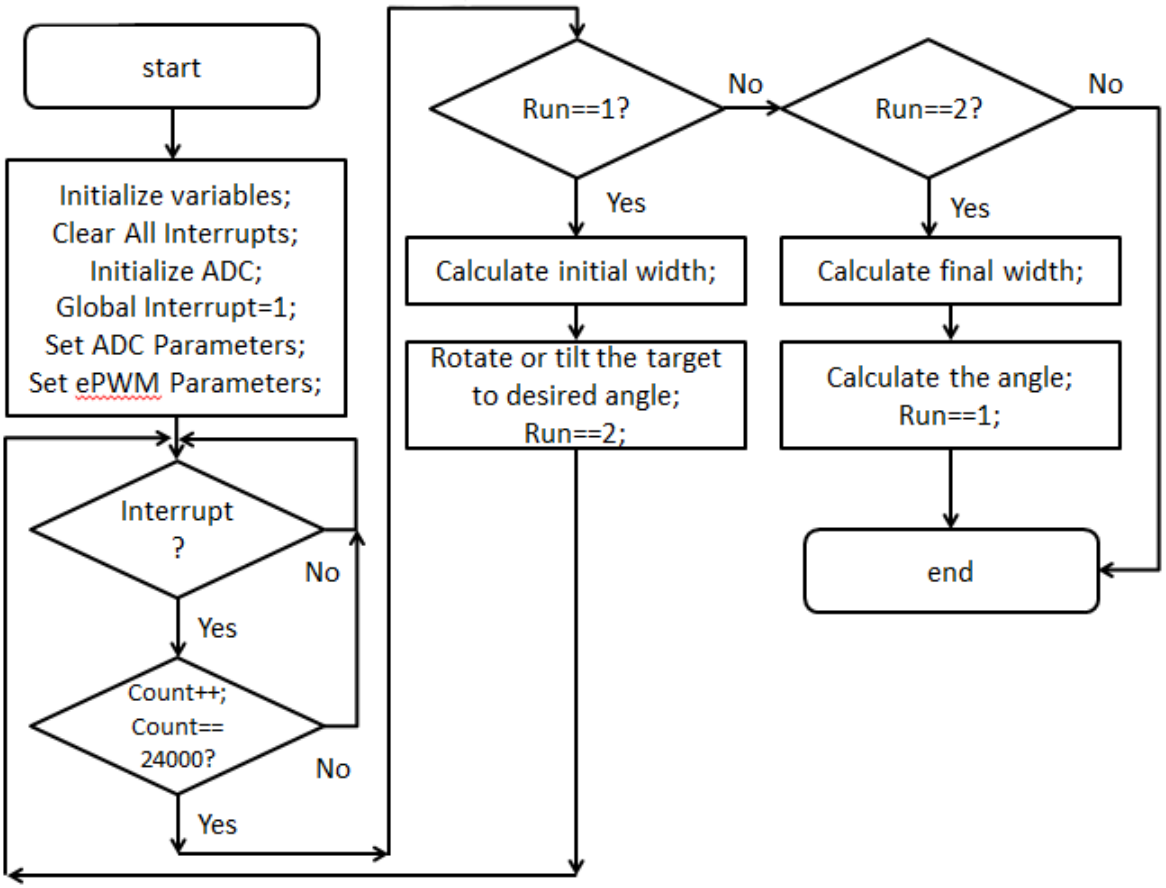

Figure 4.1: Flow Chart of the microcontroller

value is 400 thus, sampling frequency is 0.2MHz.

$$ADC Sampling frequency = \frac{Clock frequency of microcontroller (80MHz)}{ePWM timebase period}$$

Chapter 5

Data Analysis

This section summarizes all the results from the data that has been collected through experiments on flat surface at a distance of 1m.

5.1 Calibration Factor

The received time stamp of the bar pattern is a function of various system parameters, such as, scan length, scan frequency and microcontroller master clock. Interpretation of the timing information requires determination of a system dependent calibration factor, or a synchronization of the microcontroller and the scan frequency.

The bar pattern with four bars having 4mm, 5mm, 6mm, and 7mm width line respectively, was printed vertically on the flat surface once with 0^0 and then with 45^0 angle from the vertical as shown in the Figure 5.1(a) and 5.1(b).

The synchronization is obtained by making two independent measurements of the line width of each bar. The first method uses an oscilloscope(or logic analyzer) and the second uses the microcontroller. Both the measured values

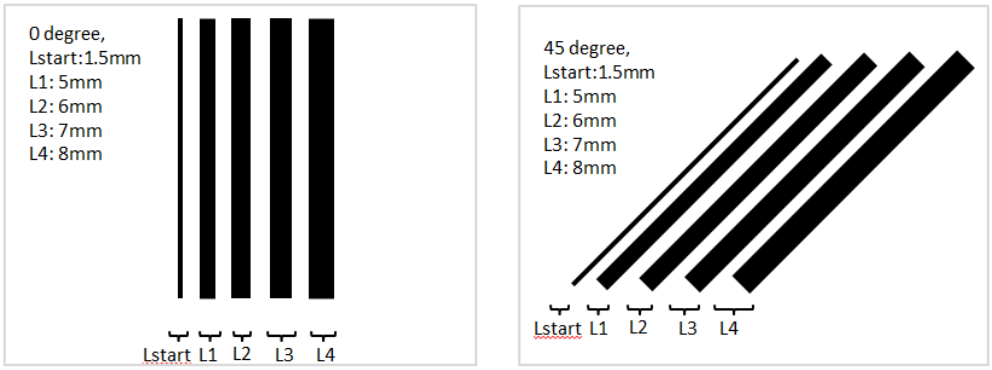

(a) Bar Pattern 1 at 0^0 (b) Bar Pattern 2 at 45^0

Figure 5.1: Bar Patterns used to find the calibration factor are shown in (a) and (b)

(a) Calibration factor at 0^0

Actual Width(mm)	**Observed width through CRO(mm)**	**Observed width through Software(mm)**	**Correction factor**
5	3.41	1.67	2.99
6	3.93	1.87	3.20
7	4.59	2.21	3.12
8	5.48	2.65	3.02

(b) Calibration factor at 45^0

Actual Width(mm)	**Observed width through CRO(mm)**	**Observed width through Software(mm)**	**Correction factor**
5	4.81	2.43	2.90
6	5.57	2.66	3.18
7	6.55	3.04	3.02
8	8.75	4.19	2.69

Table 5.1: Calculations for calibration factor at 0^0 and 45^0 angle from the vertical axis of the bar pattern as shown in figure 5.1(a) and 5.1(b) are shown in table (a) and (b),respectively

are compared to the actual bar width printed on the flat surface and calibration

factor is determined. Table 5.1(a) and 5.1(b) shows the data obtained during the experiment.

Initially, the scanning mirror is operated at 131Hz frequency, so full scan period is 7.6ms. Since only one scan is considered, so half scan period is 3.8ms. Scan length is 106mm (measured manually). From this scan velocity is determined to convert the measured pulse width in μs through microcontroller to mm. A correction factor of 3.0063 is found by averaging the correction factors in the table 5.1 at 45^0 as the measurements has been done with that bar pattern.

5.2 Experimental procedure: flat surface

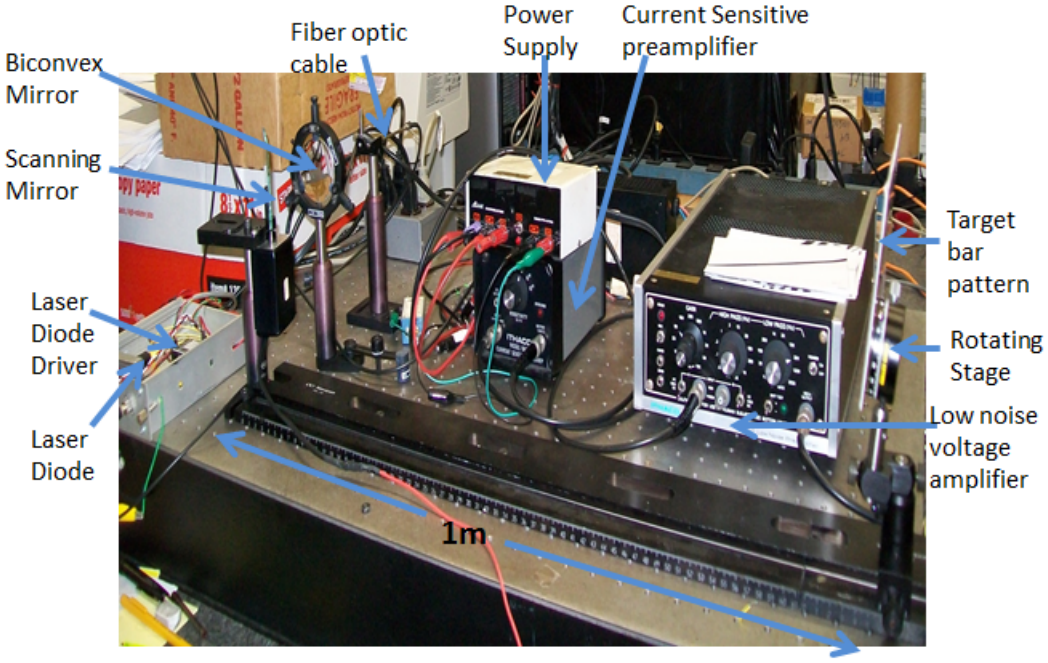

Figure 5.2: Experiment setup for flat surface rotation angle measurement

The barcode pattern with quiet zone, start(stop) line, and one line at 45^0 as previously presented in Figure 3.21 is printed on the white paper using laser printer and used in the system as shown in the Figure 5.2. The paper is taped on the surface of the board and rotated by using a manual rotating stage with a two degree angle resolution. Scanner will scan the surface straight ahead toward the surface. The test is done at 1 meter distance to prove the system can measure the rotating angle. The Figure 5.2 illustrates how the components are set up.

5.3 Setup and result analysis for flat surface rotation angle measurement

The primary purpose of the angular measurement is to measure small changes in the rotation, of the order of 1mrad at a distance of 1m. In order to facilitate this measurement, scan data at two rotation states, initial corresponding to absolute angle θ_I and final corresponding to θ_F, is recorded. From the recorded scans the two corresponding time widths T_I and T_F are computed by averaging over ten scans. The two time values are used to compute the measured change in angle, $\Delta\theta_m$. In general, the accuracy of the measured angular change is a function of average angle $\bar{\theta} = \frac{\theta_I+\theta_F}{2}$. Figure 5.3 summarizes the accuracy of measured angular change for expected angular changes angle of $\pm 2^0$, $\pm 4^0$, and $\pm 6^0$. The solid line in the Figure 5.3 indicated perfect measurement. The dashed line represents a linear fit for the measured data indicating angular resolution of $\pm 0.5^0$, for every 2^0 change over the range from 39^0 to 51^0.

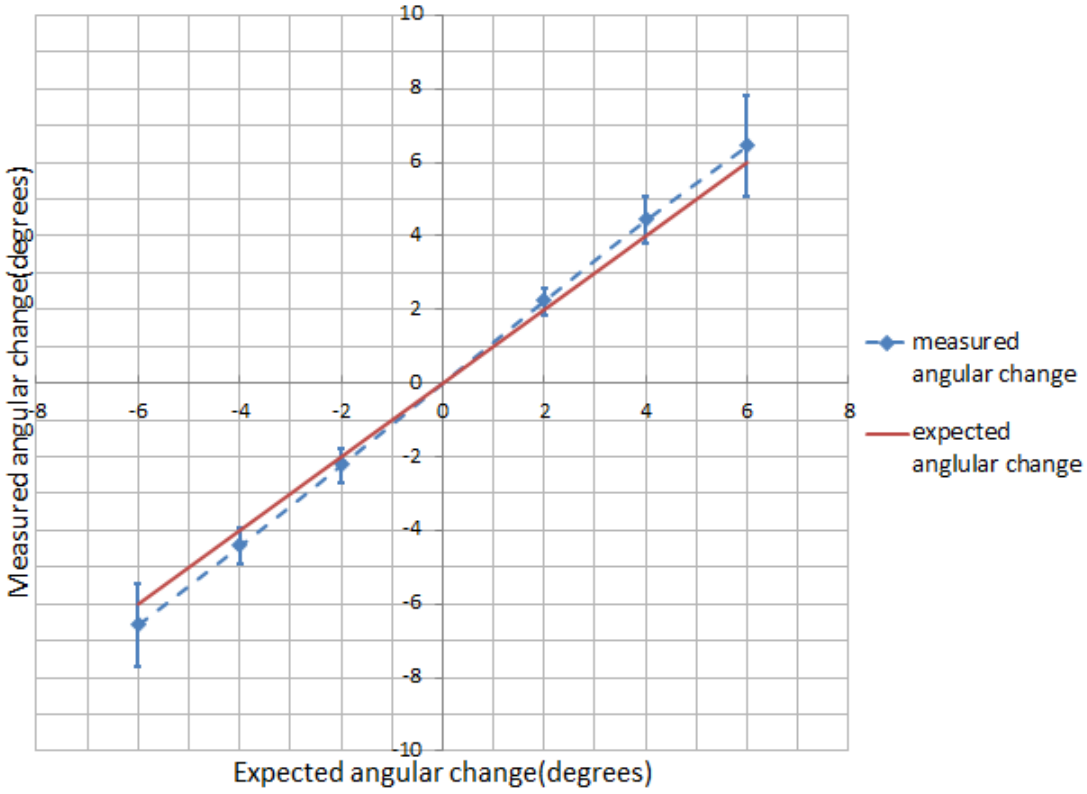

Figure 5.3: Comparison of expected and measured angle change (θ_I-θ_F) for flat surface

5.3.1 Absolute Angle Measurement

Absolute angle can be measured as described in the chapter 2. Figure 5.4 shows the very good agreement between the measured angles in the range of 60^0 to 80^0. It should be noted that the error bars are smaller than the symbols. The measured accuracy is better than 0.1^0 for 60^0 angle and increases to 0.007^0 for 80^0 angle. The center angle is set to be 70^0, therefore $\pm 10^0$ in the resolution of two degree is measured.

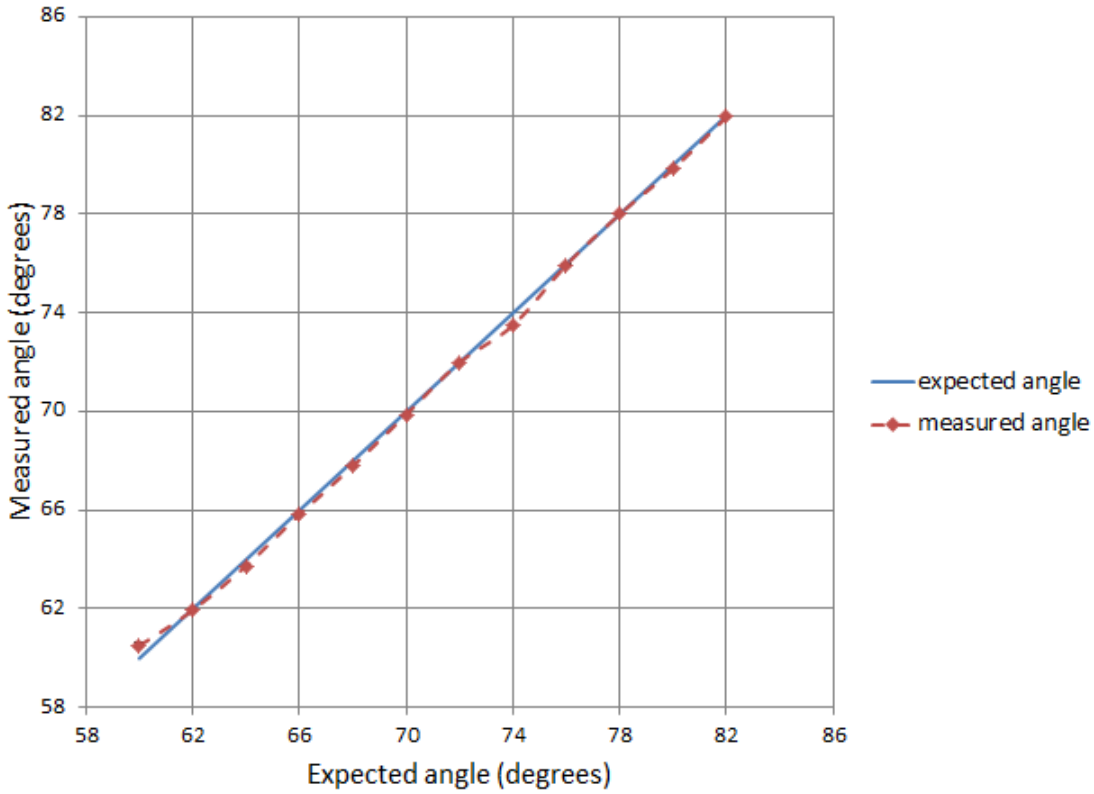

Figure 5.4: Flat surface absolute angle measurement graph between actual angle and measured angle

5.3.2 Improvements in accuracy of measured angle as initial angle of bar pattern varies

It has been seen that angle has been calculated from measured pulse width through a cosine relation dependent upon initial angle of bar pattern from the vertical axis. The slope of the cosine graph increases as the angle increases. So that a small change in angle will produce a larger change in width as the inclination angle increases. It is evident that the larger changes can be measured easily, which is also shown in graph 5.5 in which an angle change of 2^0

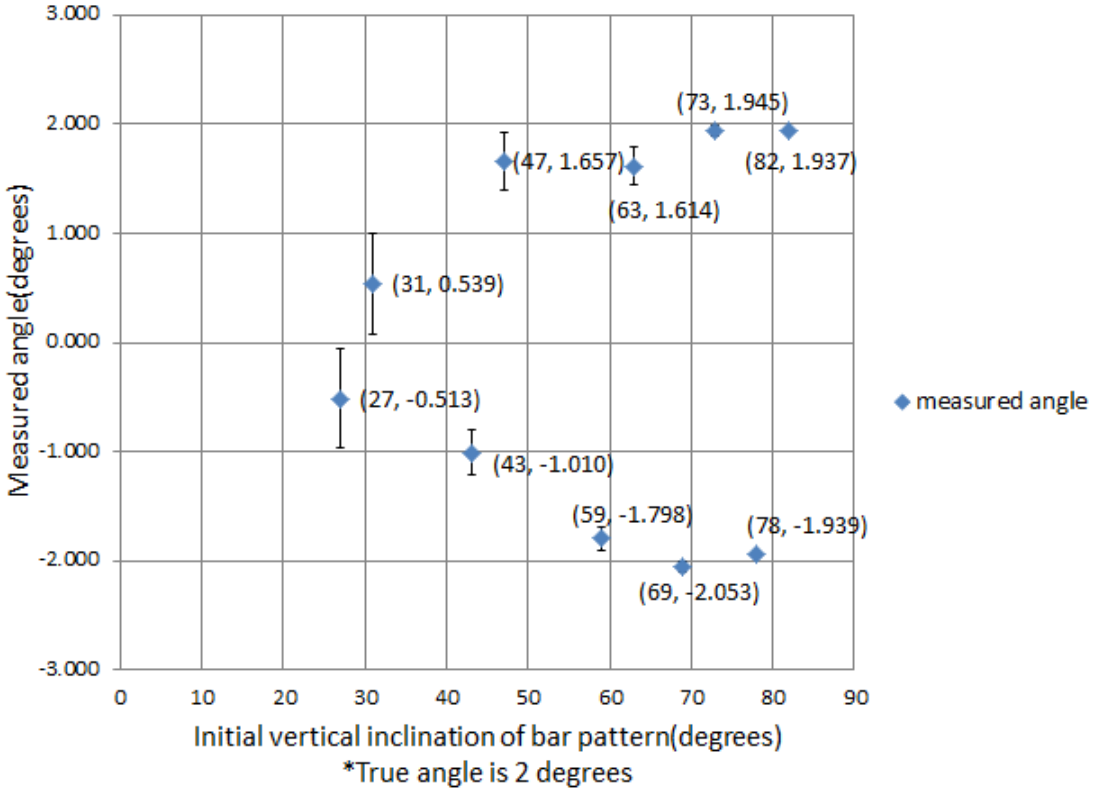

Figure 5.5: Flat surface angular accuracy improves as the vertical inclination angle of the bar pattern increases

is measured for different angles from the vertical axis. As the angle increases, the 2^0 angle can be measured with better accuracy. The co-ordinates in Figure 5.5 $(\theta, \Delta\theta)$ corresponds to the inclination angle and the differential change in the inclination angle. At an inclination angle of 80^0, a change of $\pm 2^0$ can be measured with an accuracy of $\pm 0.005^0$. The result is based on twenty scans, which is computed in a few milliseconds.

Chapter 6

Conclusion

The primary goal of this thesis was to fabricate a remote system for measuring angular changes of the order of few milliradians at a distance of 1m. We have successfully achieved this goal through the use of a laser scanner, photodiode and F28069 microcontroller based system. The bar patterns printed at 45^0 on the flat surface were successfully decoded to recover the rotation angle in the range of $\pm 6^0$ with a resolution better than $\pm 0.5^0$.

Accuracy for rotational angle measurement has been improved from $\pm 2^0$ to $\pm 0.5^0$ for small angles in comparison to previous work by Diachi[10].

Further, improvements in accuracy were possible by initially creating the bar pattern at oblique angles of inclination. For example, at an inclination angle of 80^0, changes in the angle covering a range of 2^0 could be measured with an accuracy of $\pm 0.005^0$. Furthermore, improvements in the range and accuracy may be possible by exploring more complex spatial patterns which could lead to higher resolution through enhanced signal processing techniques.

Bibliography

[1] J. Yuan and X.W. Long, "Ccd-area-based autocollimator for precision small-angle measurement," *Review of Scientific Instruments*, vol. 74, no. 3, pp. 13621366, Nov 2003.

[2] J. Yuan, X.W. Long, and K.Y. Yang, "Temperature-controlled autocollimator with ultrahigh angular measuring precision," *Review of Scientific Instruments*, vol. 76, no. 1, pp. 25106125112, Dec 2005.

[3] Y.J. Sohn, J.H. Kwon, and O.S. Choe, "Portable autocollimators using the laser diode and the position sensitive detector," *Review of Scientific Instruments*, vol. 69, no. 2, pp. 402–405, Sep 1998.

[4] J. Rohlin, "An interferometer for precision angle measurements," *Applied Optics*, vol. 2, no. 7, pp. 762–763, July 1963.

[5] G.D. Chapman, "Interferometric angular measurement," *Applied Optics*, vol. 13, no. 7, pp. 1646–1651, July 1974.

[6] P.S. Huang, S. Kiyono, and O. Kamada, "Angle measurement based on the internal-reflection effect: a new method," *Applied Optics*, vol. 28, no. 1, pp. 60476055, Oct 1992.

[7] Yong Liu, Cuifang Kuang, and Yulong Ku, "Small angle measurement method based on the total internal multi-reflection," *Optics and Laser Technology*, vol. 44, no. 1, pp. 13461350, Jan 2012.

[8] V. Kowasalya, C. T. Vijay, and S. P Barahm, "Measurement of small angular displacement by a modified moir technique," *Optical Engineering*, vol. 31, no. 12, pp. 2665–2667, Dec 1992.

[9] J. S. Rastegar and H. Dhadwal, "System and method for the measurement of the velocity and acceleration of the objects," Patent No. 7,233,389 United States of America, June 2007.

[10] Daichi Horimai, "Remote angular measurement of flat and cylindrical targets," M.S. thesis, Stony Brook University, Japan, May 2011.

[11] Thor Labs, *Pigtailed Laser Diode, SMF*, Thor Labs, Newton, NJ, January 2011.

[12] DL Instruments, *Ldd M Series Instruction Manual*, Wavelength Electronics, Bozeman, MT, June 1997.

[13] H. S. Dhadwal and A. P. Kurkov, "Dual-laser probe measurement of blade-tip clearance," *Journal of Turbomachinery*, vol. 121, no. 3, pp. 481–485, July 1999.

[14] General Scanning, *Open Loop Galvo Motors*, General Scanning Optical Scanners, Billerica, MA, August 2007.

[15] Texas Instruments Incorporated, *Piccolo Microcontrollers*, Texas Instruments, Texas, July 2011.

[16] Filip Tavernier and Michiel Steyaert, *High-Speed Optical Receivers with Integrated Photodiode in Nanoscale CMOS Springer*, vol. 1, Springer, Melville Library, Stony Brook, 1st edition, 2011.

[17] DL Instruments, *Model 1642 Current Sensitive Preamplifier*, DL Instruments, Ithaca, New York, June 1980.

[18] DL Instruments, *Model 1201 Programmable Voltage Preamplifier*, DL Instruments, Ithaca, New York, November 1980.

[19] Texas Instruments Incorporated, *Technical Reference Manual for F28069*, Texas Instruments, Texas, December 2011.